Transport of high-energy charged particles through spatially-intermittent turbulent magnetic fields

L. E. Chen,[1] A. F. A. Bott,[1] P. Tzeferacos,[1,2] A. Rigby,[1] A. Bell,[1] R. Bingham,[3,4] C. Graziani,[5] J. Katz,[6] M. Koenig,[7,8] C. K. Li,[9] R. Petrasso,[9] H.-S. Park,[10] J. S. Ross,[10] D. Ryu,[11] T. G. White,[1,12] B. Reville,[13] J. Matthews,[1] J. Meinecke,[1] F. Miniati,[1] E. G. Zweibel,[14] S. Sarkar,[1] A. A. Schekochihin,[1] D. Q. Lamb,[2] D. H. Froula,[6] and G. Gregori[1,2]

[1]*Department of Physics, University of Oxford, Parks Road, Oxford OX1 3PU, UK*
[2]*Department of Astronomy and Astrophysics, University of Chicago, 5640 S. Ellis Ave, Chicago, IL 60637, USA*
[3]*Rutherford Appleton Laboratory, Chilton, Didcot OX11 0QX, UK*
[4]*Department of Physics, University of Strathclyde, Glasgow G4 0NG, UK*
[5]*Argonne National Laboratory, Mathematics and Computer Science Division, Argonne, IL, USA*
[6]*Laboratory for Laser Energetics, University of Rochester, 250 E River Rd, Rochester, NY 14623, USA*
[7]*Laboratoire pour lUtilisation de Lasers Intenses, UMR7605, CNRS CEA, France*
[8]*Graduate School of Engineering, Osaka University, Suita, Osaka 565-0871, Japan*
[9]*Massachusetts Institute of Technology, 77 Massachusetts Ave, Cambridge, MA 02139, USA*
[10]*Lawrence Livermore National Laboratory, 7000 East Ave, Livermore, CA 94550, USA*
[11]*Department of Physics, School of Natural Sciences, UNIST, Ulsan 44919, Korea*
[12]*Department of Physics, University of Nevada, Reno, Nevada 89557, USA*
[13]*School of Mathematics and Physics, Queens University Belfast, Belfast BT7 1NN, UK*
[14]*Departments of Astronomy and Physics, University of Wisconsin, 475 N. Charter Street, Madison, Wisconsin 53706, USA*

Identifying the sources of the highest energy cosmic rays requires understanding how they are deflected by the stochastic, spatially intermittent intergalactic magnetic field. Here we report measurements of energetic charged-particle propagation through a laser-produced magnetized plasma with these properties. We characterize the diffusive transport of the particles experimentally. The results show that the transport is diffusive and that, for the regime of interest for the highest-energy cosmic rays, the diffusion coefficient is unaffected by the spatial intermittency of the magnetic field.

The interplay between charged particles and stochastic magnetic fields generated by plasma turbulence is crucial to understanding how cosmic rays propagate through space [1–3]. A key parameter for determining the underlying nature of charged-particle diffusion is the ratio of the particle gyroradius r_g to the correlation length ℓ_B of the magnetic turbulence. For the vast majority of cosmic rays detected at the Earth, this parameter is small. These are particles that are well confined by the Galactic magnetic field. But for cosmic rays more energetic than about 10 EeV, this parameter is larger than unity. These ultra-high-energy cosmic rays (UHECRs) are not confined to the Milky Way and are presumed to be extragalactic in origin. Identifying their sources requires understanding how they are deflected by the intergalactic magnetic field, which appears to be stochastic and spatially intermittent.

To study the propagation of cosmic rays, a theoretical framework has been developed based on direct numerical simulations of particle orbits and complemented by statistical techniques (see [4] for a review). In particular, it has been shown [5] that random, small-amplitude fluctuations of the magnetic field superimposed on a mean background field lead to diffusive particle propagation. As a result, standard (Markovian) diffusion is widely used in modeling cosmic-ray transport (e.g., [6–9]), although anomalous diffusion has been shown to occur in special cases [10–12], including resonant scattering of charged particles in spatially intermittent magnetic fields [13].

Past laboratory experiments have studied particle transport in diffuse plasmas with strong mean magnetic fields [14–17], but the regime that is relevant to UHECR transport in the intergalactic medium (IGM), i.e., a stochastic, spatially intermittent magnetic field with zero mean ($\langle \boldsymbol{B} \rangle = 0$), and under conditions of weak magnetization ($r_g \gg \ell_B$), has not been studied theoretically, numerically, or experimentally.

Here we report the results of laboratory experiments focus on this regime. We carried out these experiments at the Omega Laser Facility at the Laboratory for Laser Energetics at the University of Rochester [18]. A high-velocity, magnetized, turbulent plasma was generated (Fig. 1), employing the same platform as previously used to demonstrate dynamo amplification of magnetic fields [19, 20]. Three-dimensional simulations with the radiation-magnetohydrodynamics code FLASH [21–23] guided and informed the experimental design, including target specifications and the timing of diagnostics [19].

The platform consists of two 50 μm-thick polystyrene (CH) foils attached to a pair of 230 μm-thick CH washers, with 400 μm-diameter machined "wells" that act as collimators, placed 8 mm apart. Between the two targets we position a pair of grids, comprised of periodic 300 μm holes and 100 μm wires, placed 4 mm apart. The grid

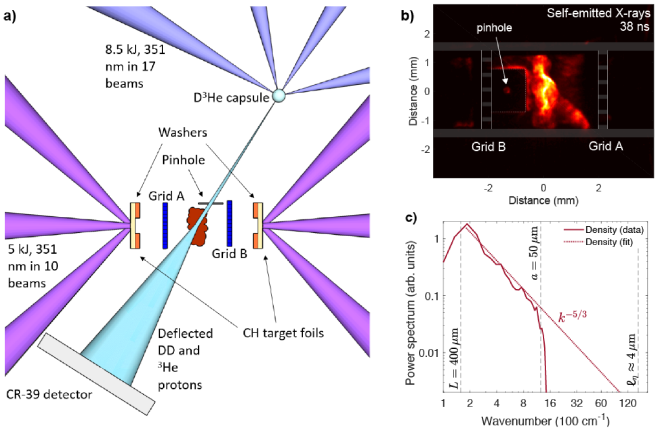

FIG. 1: **Experimental setup**. **a)** Schematic of the experimental platform, showing the target components and the configuration of the proton radiography experimental diagnostic. **b)** X-ray self-emission from the interaction region at $t = 38$ ns after the start of the laser drive. **c)** Power spectrum of the density fluctuations recovered from the fluctuations of X-ray self-emission. The resolution of the diagnostic (the size of the pinhole employed on the X-ray framing camera) is 50 μm, which is below the driving scale, but above the plasma's dissipative scales.

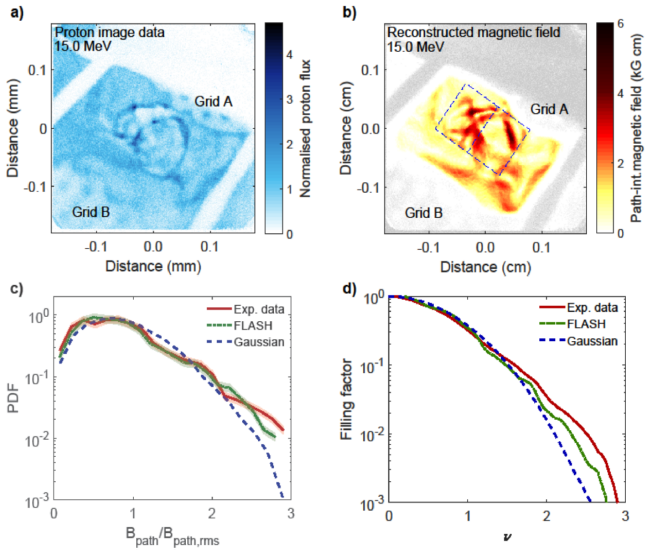

FIG. 2: **Magnetic field reconstruction. a)** 15 MeV proton radiography image of the entire interaction region at 38 ns, without pinhole shield present in the path. For clarity, the image length scales are shown without the ×28 magnification factor; with this factor, the image has dimensions of 10 cm × 10 cm. **b)** Magnitude of the two components of path-integrated magnetic field that are perpendicular to the proton beam path, reconstructed [24] from the 15 MeV proton image in a). **c)** PDF of the magnitude of the path-integrated magnetic field $B_{\rm path}$ at 38 ns. The PDF (red) is calculated using the mean of the PDFs for the two rectangular regions depicted in b); the uncertainty is derived from the standard error. The PDF of the path-integrated field arising in the FLASH simulations is also plotted (green), as is a Gaussian reference (blue) with the same RMS field strength. **d)** The fraction of area of the path-integrated magnetic field in which the field's magnitude $B_{\rm path}$ satisfies $B_{\rm path} \geq \nu B_{\rm path,rms}$, where $B_{\rm path,rms}$ is the RMS path-integrated field. This quantity is again calculated from the rectangular regions demarcated in b).

patterns are shifted to break the mirror symmetry of the system. Each foil is irradiated with 5 kJ of energy during a 10 ns pulse (10 frequency-tripled laser beams on each foil staggered in time). The drive produces two counter-propagating plasma flows, which pass through the pair of grids, meet, shear each other, and become turbulent in the central region between the two grids (the interaction region). For a detailed description of the experimental platform and the nature of the turbulence it generates, see Ref [20].

The electron density and temperature of the turbulent plasma are measured using collective Thomson scattering [25] and found to be $n_e \simeq 9\times10^{19}$ cm^{-3} and $T_e \simeq 400$ eV immediately after the formation of the turbulent region ($t \simeq 27$ ns after the start of the drive). The mean velocity ($u_{\rm flow}$) and the turbulent velocity ($u_{\rm turb}$) of the flow are also obtained by this diagnostic. Prior to collision, the counter-propagating flows reach velocities of $u_{\rm flow} \simeq 2\times10^7$ cm s^{-1}, whereas in the turbulent region at late times we measure $u_{\rm flow} \simeq 5\times10^6$ cm s^{-1} and $u_{\rm turb} \simeq 10^7$ cm s^{-1} at the driving scale of the turbulence ($L \simeq 400$ μm, set by the grid spacing).

The plasma interaction region's evolution is determined using self-emitted soft X-rays (Fig. 1b shows the plasma emission at 38 ns after the start of the laser drive). As discussed in Ref [20], fluctuations in the emissivity of such a plasma can be related to fluctuations of density [26]; the latter exhibit a Kolmogorov power-law spectrum, with driving scale L consistent with the grid spacing detailed above (Fig. 1c). The spatial extent of the interaction region over time can also be measured using the X-ray diagnostic. Further details concerning the plasma state are given in the Supplemental Material [27].

The stochastic magnetic fields amplified in the turbulent plasma [19, 20] are measured using proton radiography (Fig. 2). A 420 μm-diameter SiO_2 capsule, with a 2-μm-thick shell, is filled with 18 atm D^3He gas (6 atm ^{2}D and 12 atm ^{3}He) and is placed 10 mm away from the interaction region. The capsule is imploded using 17 beams (frequency-tripled to 351 nm, providing 270 J/beam for a 1 ns pulse) to produce 3.3 and 15 MeV fusion protons [28, 29]. The protons are recorded on the

opposite side of the capsule with a nuclear track detector (CR-39) film pack, 27 cm from the plasma interaction region, achieving a magnification of $\times 28$. Fig. 2a shows a proton radiograph of the plasma corresponding to the same time as the X-ray image in Fig. 1b. The presence of strong inhomogeneities in the proton flux and the stochastic, non-regular morphology of the structures is due to protons being deflected by strong, tangled magnetic fields. From the flux inhomogeneities observed in the proton image, the experimental radiographs can be inverted [24, 30] to recover two components of the path-integrated magnetic field (Fig. 2b). Using the measured spatial extent of the interaction region, it can be shown that the measured path-integrated magnetic field corresponds to a root mean square (RMS) value $B_{rms} \simeq$ 65-80 kG, with a typical correlation length $\ell_B \approx 90\,\mu$m.

The statistics of the path-integrated magnetic field is expected to deviate from Gaussian as a result of the spatial intermittency. To quantify this, we show in Fig. 2c that the probability density function (PDF) of the magnitude of the path-integrated field has an extended tail. This is also illustrated by the field's filling factor (Fig. 2d). Since the path-integrated magnetic field is spatially intermittent, it follows that the field itself must also be spatially intermittent. Indeed, the PDF of the magnetic field strength in the FLASH simulations exhibits an exponential tail. The simulations also demonstrate that the deviation from Gaussian statistics is much more pronounced in the three-dimensional true fields than the two-dimensional path-integrated field [27]. Such non-Gaussian, spatially-intermittent magnetic fields are expected to arise when the fluctuation dynamo is operating [31].

To characterize the transport of particles through the turbulent plasma, we modified our experimental platform to introduce a collimated proton beam. The collimation was achieved by placing a 200-μm-thick aluminum shield between the D^3He capsule and the interaction region, with a 300-μm-diameter pinhole (shown in Fig. 1a). The pinhole imprint is then recorded on the detector plane, as shown in Fig. 3. The proton-beam imprints appear deformed and broadened due to the interaction of the protons with the turbulent magnetized plasma. The proton-beam imprint contours are shown in Figs. 4a and 4b. The corresponding deflection velocities, $\Delta v_\perp$, as interpreted from the scattering angle $|\Delta v_\perp|/V$, where V is the proton-beam speed, are shown in Fig. 4c. Using the synthetic proton radiography diagnostic of the FLASH code [19] we also post-processed the FLASH simulation results to recover proton trajectories and the resultant transverse deflections. These are in good agreement with the experimental measurements (Fig. 4c).

The velocity deflection $\Delta v_\perp$ due to magnetic fields scales independently of velocity, whereas the velocity deflection due to electric fields scales as $\propto 1/V$ [27]. The near-equality of the deflection velocities of the two proton species, evident in Fig. 4c, suggests that scattering is predominantly due to magnetic fields. While there are many other possible processes that could lead to scattering of a charged-particle beam passing through a turbulent plasma, for our experiment we argue that these other processes are negligible, on account of the low density of the plasma and the large speed of the protons compared to driving-scale plasma motions. Detailed calculations and descriptions of possible electric field effects are given in the Supplemental Material [27].

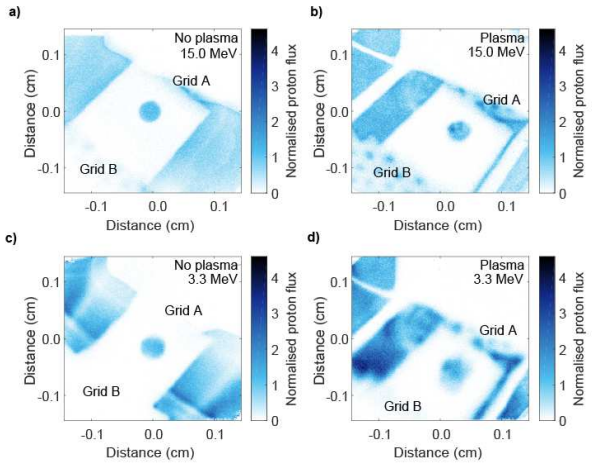

FIG. 3: **Proton pinhole images.** Radiographs obtained on the CR-39 film pack with proton energies of **a)** 15 MeV, with no plasma in the interaction region, and **b)** 15 MeV, with a turbulent plasma in the interaction region. **c)** Same as **a)** but for the 3.3 MeV protons. **d)** Same as **b)** but for the 3.3 MeV protons. The pinhole shield is clearly seen to block most of the incoming proton flux from the capsule and, in the case where no plasma was present (**a)** and **c)**), it produces a fixed 300 μm diameter beam of 3.3 and 15 MeV protons that passes through to the detector. For the case when a plasma is present in the interaction region (**b)** and **d)**), the beam is deformed and broadened before reaching the detector.

From our experimental measurement of $\Delta v_\perp$, we can calculate the associated scattering frequency in velocity-space, $\nu \sim (\Delta v_\perp/V)^2/\tau$, where $\tau = \ell_i/V$ is the transit time of the particles through the plasma and ℓ_i is the scale of the interaction region as inferred from the X-ray images. For a plasma with dimensions much bigger than the proton mean free path $\lambda \equiv V/\nu$, our results imply an isotropic spatial diffusion coefficient $\kappa \sim V^2/\nu = \ell_i V^3/(\Delta v_\perp)^2$. Since κ/V^3 is constant in our experiment (Fig. 4d), this implies $(\Delta v_\perp)^2 \propto \ell_i \propto \tau$. This is consistent with a normal (Markov) spatial diffusion [4, 32, 33].

Since the charged particle transport is consistent with normal spatial diffusion through a stochastic field, we can compare the experimental results to theoretical pre-

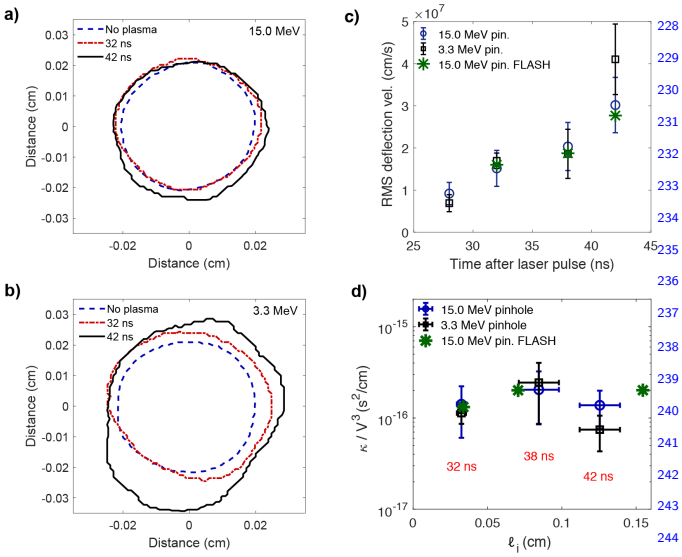

FIG. 4: **Diffusive scattering of the proton beam.** Contours of the beam imprint on the CR-39 plate for **a)** 15 MeV protons and **b)** 3.3 MeV protons, taken with different delay times after the start of the drive beams. **c)** The RMS transverse deflection velocity acquired by the proton beam, calculated using the contour analysis of the pinhole image (for both proton species), and evaluated for the FLASH simulations. **d)** Measured spatial diffusion coefficient as a function of the plasma interaction length, as determined from the X-ray self-emission images and the 15 MeV pinhole synthetic radiographs from the FLASH simulations.

dictions from a random walk process. Using characteristic, experimentally measured values for the plasma properties corresponding to $t = 38$ ns after the start of the drive, we take the size of the interaction region to be $\ell_i \simeq 0.08\,\mathrm{cm}$, the typical magnetic field strength $B_{\rm rms} \simeq 75\,\mathrm{kG}$, and the correlation length $\ell_B \approx 90\,\mu\mathrm{m}$. For the case of normal diffusion, a random-walk argument gives $\Delta v_\perp \approx q_e B_{\rm rms}\sqrt{\ell_i \ell_B}/m_p \simeq 1.9\times10^7\,\mathrm{cm\,s^{-1}}$ (see [27]) where m_p is the mass of a proton. This value is consistent with the measured RMS deflection velocity (Fig. 4c). Further, since the values of V, $B_{\rm rms}$, and the power spectrum of the magnetic energy (and therefore the value of ℓ_B) do not change in the experiment after the magnetic-field amplification saturates [19, 20, 27], the random walk model also predicts a constant $\kappa/V^3 \sim m_p^2/(q_e B_{\rm rms})^2 \ell_B \simeq 2\times10^{-16}\,\mathrm{s^2\,cm^{-1}}$, in quantitative agreement with the experimental results (Fig. 4d).

For isotropic statistics and $r_g/\ell_B \gg 1$, the proton mean free path is $\lambda \simeq 10^4\,\mathrm{cm}$. In this regime, theory [34] and simulations [33] predict that the ratio of the proton mean free path and the correlation length ℓ_B scales as $\lambda/\ell_B \propto (r_g/\ell_B)^2$. Since $r_g/\ell_B \simeq 830$ for the 15 MeV and $\simeq 390$ for the 3.3 MeV protons, we can use this scaling to extrapolate from [33] a ratio $\lambda/\ell_B \simeq 0.3 - 1\times10^6$, which is consistent with the experimental values that we obtain within a factor of unity ($\lambda/\ell_B \simeq 10^6$ in the experiment). This agreement provides experimental evidence of the $\lambda \propto r_g^2/\ell_B$ scaling in the large-r_g/ℓ_B regime. More importantly, our results demonstrate that the diffusion of charged particles in the large-r_g/ℓ_B regime is not affected by the spatial intermittency of the stochastic magnetic fields, validating Gaussian-random-field models typically employed to study cosmic-ray propagation, e.g., [6–9].

One possibly counter-intuitive aspect of our results is the success of the random-walk model for deriving estimates and scalings for $\Delta v_\perp$ in spite of the fact that the number of interactions $N_0 \sim \ell_i/2\ell_B$ experienced by an individual particle is not particularly large: for example, at the 32 ns delay (for which $\ell_i \approx 330\,\mu$m), we find $N_0 \approx 2$. Thus, it is not the case in our experiment that each individual beam proton always encounters a great number of uncorrelated magnetic structures. In the experiment, because the cross-sectional area A of the collimated pinhole beam is greater than the characteristic structure size and, therefore, the beam protons interact with a larger number of structures $N \sim A\ell_i/(2\ell_B)^3 > N_0$, it follows that the average value of $\Delta v_\perp$ for the beam obeys a scaling with ℓ_i that is much closer to the random-walk model's prediction than would reliably be measured for an individual particle. These claims are illustrated numerically in the Supplemental Material [27].

These results validate the use of standard diffusion theory in modeling the transport of UHECRs in the IGM, e.g., [6–9]. This is useful in view of the increased interest in such modelling motivated by the recent detection by the Pierre Auger Observatory of a significant anisotropy in the arrival directions of cosmic rays of energy above 8 EeV [35].

The research leading to these results has received funding from the European Research Council under the European Community's Seventh Framework Programme (FP7/2007-2013) / ERC grant agreements no. 256973 and 247039, the U.S. Department of Energy under Contract No. B591485 to Lawrence Livermore National Laboratory, Field Work Proposal No. 57789 to Argonne National Laboratory, and grants no. DE-NA0002724, DE-NA0003605, and DE-SC0016566 to the University of Chicago. We acknowledge support from the National Science Foundation under grants PHY-1619573 and AST-1616037 and from Department of Energy Cooperative Agreement No. DE-NA0001944 to the University of Rochester. Awards of computer time were provided by the U.S. Department of Energy ASCR Leadership Computing Challenge (ALCC) program. This research used resources of the Argonne Leadership Computing Facility at Argonne National Laboratory, which is supported by the Office of Science of the U.S. Department of Energy under contract DE-AC02-06CH11357. Support from AWE plc., the Engineering and Physical Sci-

ences Research Council (grant numbers EP/M022331/1, EP/N014472/1 and EP/P010059/1) and the Science and Technology Facilities Council of the United Kingdom is also acknowledged, as well as funding from grants 2016R1A5A1013277 and 2017R1A2A1A05071429 of the National Research Foundation of Korea. J. Matthews, A. Bell and G. Gregori would like to thank Prof. Katherine Blundell (University of Oxford) for stimulating discussions on cosmic-ray measurements.

[1] A. W. Strong, I. V. Moskalenko, and V. S. Ptuskin, Annual Review of Nuclear and Particle Science **57**, 285 (2007).
[2] E. G. Zweibel, Physics of Plasmas **20**, 055501 (2013).
[3] R. Schlickeiser, Physics of Plasmas **22**, 091502 (2015).
[4] A. Shalchi, *Nonlinear Cosmic Ray Diffusion Theories* (Springer, 2009).
[5] J. R. Jokipii, The Astrophysical Journal **146**, 480 (1966).
[6] K. Kotera and M. Lemoine, Physical Review D **77**, 123003 (2008).
[7] Globus, N., Allard, D., and Parizot, E., A&A **479**, 97 (2008).
[8] N. Globus and T. Piran, The Astrophysical Journal **850**, L25 (2017).
[9] N. Globus, T. Piran, Y. Hoffman, E. Carlesi, and D. Pomarde, Monthly Notices of the Royal Astronomical Society **484**, 4167 (2019).
[10] J. R. Jokipii and E. N. Parker, The Astrophysical Journal **155**, 799 (1969).
[11] B. Reville, S. O'Sullivan, P. Duffy, and J. G. Kirk, Monthly Notices of the Royal Astronomical Society **386**, 509 (2008).
[12] A. Lazarian and H. Yan, The Astrophysical Journal **784** (2014).
[13] A. Shukurov, A. P. Snodin, A. Seta, P. J. Bushby, and T. S. Wood, Astrophys. J. **839**, L16 (2017).
[14] K. Gustafson, P. Ricci, I. Furno, and A. Fasoli, Physical Review Letters **108**, 035006 (2012).
[15] J. K. Anderson, A. F. Almagri, D. J. Den Hartog, S. Eilerman, C. B. Forest, J. J. Koliner, V. V. Mirnov, L. A. Morton, M. D. Nornberg, E. Parke, J. A. Reusch, J. S. Sarff, J. Waksman, V. Belykh, V. I. Davydenko, A. A. Ivanov, S. V. Polosatkin, Y. A. Tsidulko, L. Lin, D. Liu, G. Fiksel, H. Sakakita, D. A. Spong, and J. Titus, Physics of Plasmas **20**, 056102 (2013).
[16] I. Furno, F. Avino, A. Bovet, A. Diallo, A. Fasoli, K. Gustafson, D. Iraji, B. Labit, J. Loizu, S. H. Müller, G. Plyushchev, M. Podestà, F. M. Poli, P. Ricci, and C. Theiler, Journal of Plasma Physics **81**, 345810301 (2015).
[17] A. Bovet, A. Fasoli, P. Ricci, I. Furno, and K. Gustafson, Physical Review E **91**, 041101 (2015).
[18] T. Boehly, D. Brown, R. Craxton, R. Keck, J. Knauer, J. Kelly, T. Kessler, S. Kumpan, S. Loucks, S. Letzring, F. Marshall, R. McCrory, S. Morse, W. Seka, J. Soures, and C. Verdon, Optics Communications **133**, 495 (1997).
[19] P. Tzeferacos, A. Rigby, A. Bott, A. R. Bell, R. Bingham, A. Casner, F. Cattaneo, E. M. Churazov, J. Emig, N. Flocke, F. Fiuza, C. B. Forest, J. Foster, C. Graziani, J. Katz, M. Koenig, C.-K. Li, J. Meinecke, R. Petrasso, H.-S. Park, B. A. Remington, J. S. Ross, D. Ryu, D. Ryutov, K. Weide, T. G. White, B. Reville, F. Miniati, A. A. Schekochihin, D. H. Froula, G. Gregori, and D. Q. Lamb, Physics of Plasmas **24**, 041404 (2017).
[20] P. Tzeferacos, A. Rigby, A. Bott, A. R. Bell, R. Bingham, A. Casner, F. Cattaneo, E. M. Churazov, J. Emig, F. Fiuza, C. B. Forest, J. Foster, C. Graziani, J. Katz, M. Koenig, C. K. Li, J. Meinecke, R. Petrasso, H. S. Park, B. A. Remington, J. S. Ross, D. Ryu, D. Ryutov, T. G. White, B. Reville, F. Miniati, A. A. Schekochihin, D. Q. Lamb, D. H. Froula, and G. Gregori, Nature Communications **9**, 591 (2018).
[21] B. Fryxell, K. Olson, P. Ricker, F. Timmes, M. Zingale, D. Lamb, P. MacNeice, R. Rosner, J. Truran, and H. Tufo, The Astrophysical Journal Supplement Series **131**, 273 (2000).
[22] A. Dubey, K. Antypas, M. Ganapathy, L. Reid, K. Riley, D. Sheeler, A. Siegel, and K. Weide, Parallel Computing **35**, 512 (2009).
[23] P. Tzeferacos, M. Fatenejad, N. Flocke, C. Graziani, G. Gregori, D. Q. Lamb, D. Lee, J. Meinecke, A. Scopatz, and K. Weide, High Energy Density Physics **17**, 24 (2015).
[24] A. F. A. Bott, C. Graziani, P. Tzeferacos, T. G. White, D. Q. Lamb, G. Gregori, and A. A. Schekochihin, Journal of Plasma Physics **83**, 905830614 (2017).
[25] J. Katz, R. Boni, C. Sorce, R. Follett, M. J. Shoup, and D. H. Froula, Review of Scientific Instruments **83**, 10349 (2012).
[26] E. Churazov, A. Vikhlinin, I. Zhuravleva, A. Schekochihin, I. Parrish, R. Sunyaev, W. Forman, H. Böhringer, and S. Randall, Monthly Notices of the Royal Astronomical Society **421**, 1123 (2012).
[27] See Supplemental Material at [URL will be inserted by publisher] for a detailed characterization of the plasma state, the proton radiography analysis, and a full description of the FLASH simulations.
[28] C. K. Li, F. H. Seguin, J. A. Frenje, J. R. Rygg, R. D. Petrasso, R. P. J. Town, P. A. Amendt, S. P. Hatchett, O. L. Landen, A. J. MacKinnon, P. K. Patel, V. A. Smalyuk, T. C. Sangster, and J. P. Knauer, Physical Review Letters **97**, 135003 (2006).
[29] N. L. Kugland, D. D. Ryutov, C. Plechaty, J. S. Ross, and H. S. Park, Review of Scientific Instruments **83**, 101301 (2012).
[30] C. Graziani, P. Tzeferacos, D. Q. Lamb, and C. Li, Review of Scientific Instruments **88**, 123507 (2017).
[31] A. A. Schekochihin, S. C. Cowley, S. F. Taylor, J. L. Maron, and J. C. McWilliams, The Astrophysical Journal , 276 (2004).
[32] V. N. Tsytovich, *Theory of Turbulent Plasma* (Consultants Bureau, 1977).
[33] P. Subedi, W. Sonsrettee, P. Blasi, D. Ruffolo, W. H. Matthaeus, D. Montgomery, P. Chuychai, P. Dmitruk, M. Wan, T. N. Parashar, and R. Chhiber, The Astrophysical Journal **837**, 140 (2017).
[34] A. Dolginov and I. Toptygin, Journal of Experimental and Theoretical Physics **24**, 1195 (1967).
[35] The Pierre Auger Collaboration, Science **357**, 1266 (2017).